A microfluidic gas damper for stabilizing gas pressure in portable microfluidic systems

Xinjie Zhang, Zhixian Zhu, Nan Xiang,[a] and Zhonghua Ni[a]
School of Mechanical Engineering, and Jiangsu Key Laboratory for Design and Manufacture of Micro-Nano Biomedical Instruments, Southeast University, Nanjing 211189, China

(Received 5 September 2016; accepted 18 October 2016; published online 28 October 2016)

Pressure fluctuations, which invariably occur in microfluidic systems, usually result in the unstable fluid delivery in microfluidic channels. In this work, a novel microfluidic gas damper is proposed and applied for providing stable fluid-driving pressures. Then, a pressure-driven flow setup is constructed to investigate the gas damping characteristics of our damper. Since the pressure-driven flow setup functions as a resistor-capacitor low-pass filter, the damper significantly decreases the amplitude of the input pressures via self-regulating its pneumatic resistance. In addition, the gas volume and pressure frequency are found to have direct effects on the pressure fluctuations. The practical application of the gas damper is examined through a portable pressure-driven system, which consists of an air blower, a gas damper, and a centrifuge tube. By periodically pressing the air blower, precise flow rates with low throughput ($\sim$9.64 μl min^{-1}) and high throughput ($\sim$1367.15 μl min^{-1}) are successfully delivered. Future integration of our microfluidic gas damper with miniaturized pressure generators (e.g., peristaltic or pressure-driven micropumps) can fully exploit the potential of the gas damper for low-cost, portable microfluidics where stable pressures or flow rates are required. *Published by AIP Publishing*. [http://dx.doi.org/10.1063/1.4966646]

I. INTRODUCTION

Sample injection is an inevitable segment in nearly all microfluidic applications. The accuracy and stability of the microfluidic sample injection would directly influence the functional performance of microfluidic devices. Until now, commercial instruments (e.g., syringe pumps and other mechanical pumps) have still been the most widely employed schemes for microfluidic injection.[1–5] Benefiting from the sophisticated mechanism and sensor feedback, the displaced volume in these pumps can be controlled accurately. However, the bulky volumes and high costs make these commercial instruments not applicable for portable integrations.

In attempts to control microfluids in a low-cost and portable manner, various techniques for driving liquid flows in microchannels have been proposed, such as compressed gas driven,[6,7] electro-osmotic flow,[8,9] capillary flow,[10,11] hydrostatic force,[12,13] and centrifugal force.[14,15] Although these previously reported techniques show acceptable performances in flow control in microchannels, they are either too complex due to the requirement of external equipments or limited in terms of sample types and volumes. In addition, the flow-rates delivered using these techniques are usually unstable, which directly limits the employment of these techniques in such applications where stable flows are required. Therefore, integration of the technique employed with an additional flow control component is necessary for some microfluidic applications with precise fluid deliveries, for example, clinical drug infusion,[16,17] biological cell isolation, and analysis.[18–21]

[a]Authors to whom correspondence should be addressed. Electronic addresses: nan.xiang@seu.edu.cn and nzh2003@seu.edu.cn. Tel.: +86-025-52090518, Fax: +86-025-52090501.

With the widespread adoption of the multilayer soft lithography technique in recent years, microfluidic devices integrated with polydimethylsiloxane (PDMS) monolithic valves have shown the capability of performing flow controls according to designated schemes. By actively actuating the elastic membranes or disk components inside of the control chambers, fluid flows through open microchannels can effectively be stopped by blocking the channel cross-sections.[22,23] The typical applications are micropumps and microvalves, which generally act as the integrated power sources or the flow regulators in many microfluidic devices.[24–27] Due to their appealing advantages in flexible and precise flow control, they show a strong potential for large-scale microfluidic integrations.[28–30] However, the heavy dependence on external actuation makes these devices costly. Although there are some passive devices reported previously, they face the constraints on constant flow regulations in relatively high threshold pressures (>15 kPa),[31–33] which are incompliant with low-pressure generators.[34,35]

In this work, we propose a novel concept of a microfluidic gas damper, which can be applied for stabilizing gas pressure in the disposable microfluidic systems at extremely low source pressures (<3 kPa). Different from the previously reported flow control techniques, our work provides another line of thinking to stabilize the pneumatic pressure source for smooth fluid delivery in the downstream microfluidic device by employing a gas damper in the pressure-driven system. To demonstrate the functionality of our gas damper, we first illustrate the design concept of the damper and depict the working principle of the device via a set of numerical simulations. Then, methods and experiments for characterizing the pressure damping functionality of the damper in the pressure-driven setup are demonstrated. We also investigate the key factors (i.e., gas volume size, source pressure frequency) that directly influence the amplitudes of output pressures. In the end, practical applications of the damper for achieving two significantly different flow-rate outputs are studied.

II. RESULTS AND DISCUSSION

A. Design concept and characterization of microfluidic gas damper

The design concept of our microfluidic gas damper can be interpreted as a variable gas resistor, which changes its pneumatic resistance automatically with the variation of input pressure. The schematic structure of the gas damper is shown in Figure 1(a). The device consists of two detour channels, a through channel and two elastic membranes. The dead ends of the two detour channels are aligned at the top and bottom sides of the through channel to form two hollow cavities (left inset of Figure 1(a)). When gas pressure is applied to the inlet of the device, the pneumatic force would be accumulated in the dead ends of the detour channels to actuate the membranes deforming towards each other, thus decreasing the cross-sectional area of the through channel at the intersection (the right inset of Figure 1(a)). Because the pneumatic resistance of the device is directly determined by the cross-sectional area of the through channel, the abruptly increased gas pressure will also dramatically increase the resistance of the device. Therefore, the pressure fluctuations from the power source can be effectively damped.

In order to illustrate the working principle of our gas damper more clearly, numerical simulations concerning the gas damping process were performed (Figure S1(a), supplementary material). The simulation results in Figure 1(b) show that when the inlet pressure of the damper is increased, the membranes would be deformed to contact each other, which leads to the decrease of the output pressure. In addition, both the simulations and the experiments show that the output pressures of the device with membranes (i.e., damper) increase slowly with the increase of the inlet pressures, while the linearly increased pressures are found in the device without membranes (Figures S1(b)–S1(c), supplementary material). These results demonstrate the significant gas damping characteristics of our damper.

To characterize the pressure damping performances of our gas damper, a pressure-driven flow setup was constructed to measure the output pressures in the downstream of the damper (Figure 1(c)). The working mechanism of the setup can be estimated as the equivalent electric circuit model of a classical resistor-capacitor (RC) low-pass filter (see Figure 1(d), where voltages p_s and p_o represent, respectively, the input and output gas pressure of the setup, resistor R and capacitor C represent the gas damper and the sample reservoir in the gas circuit, and load

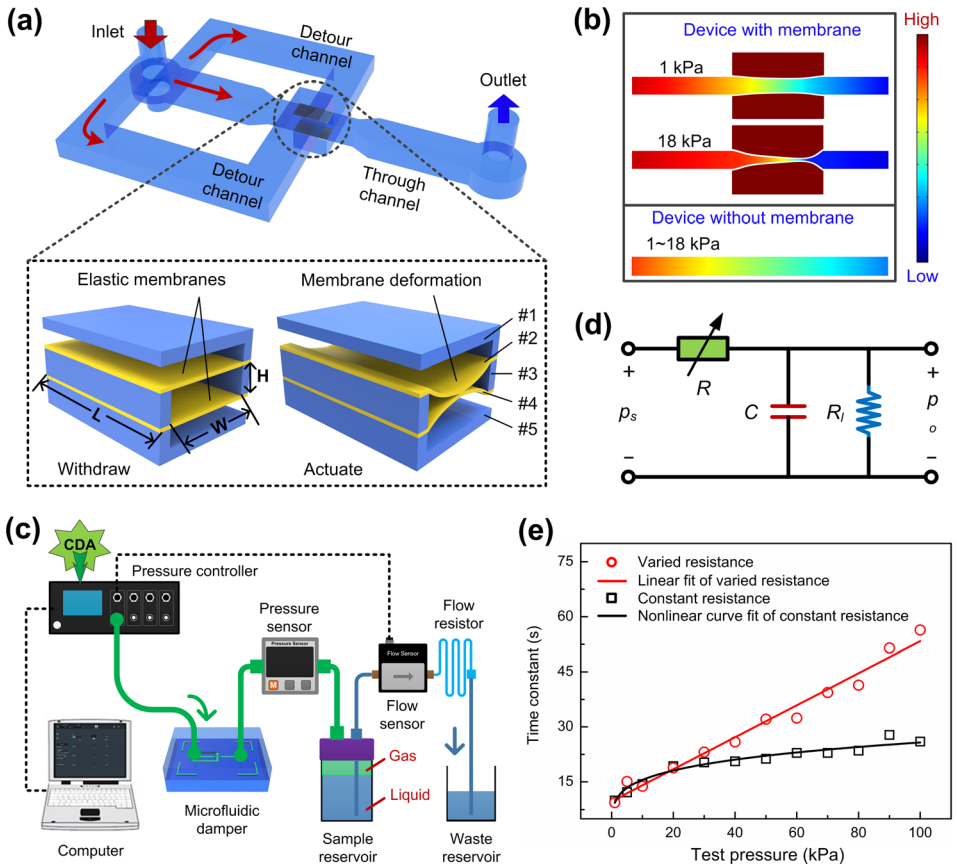

FIG. 1. Design concept of the microfluidic gas damper and the equivalent electric circuit model for the pressure-driven flow setup. (a) Schematic structure of the gas damper. Inset figures show the normally open (withdraw) and the working status (actuate) of the damper. (b) Simulated pressure distributions in the A-A section in supplementary material Figure S1a. (c) Experimental setup for characterizing the gas damping effect. (d) Equivalent electric circuit model of a resistor-capacitor (RC) low-pass filter for the constructed pressure-driven setup. (e) Time constants of the gas filling in an outlet-sealed reservoir under different test pressures from 1 kPa to 100 kPa.

resistor R_l denotes the flow resistor in the liquid circuit). In the RC low-pass filter, the high-frequency signals in the input voltage can be effectively removed so that the output voltage becomes very smooth. The amplitude A of the output voltage p_o in the electric circuit of the RC low-pass filter can be given as

$$A = \frac{1}{\sqrt{1 + (2\pi f \tau)^2}}, \tag{1}$$

where f is the frequency of the input voltage, which represents the pulsation frequency of the input gas pressure in the pressure-driven flow setup, and τ is the time constant (i.e., the time of output pressure to achieve constant), which reflects the damping capability of the setup. The value of time constant τ can be calculated as

$$\tau = RC. \tag{2}$$

Substituting the Equation (2) into Equation (1) yields the detailed expression of the amplitude of output voltage as

$$A = \frac{1}{\sqrt{1 + (2\pi fRC)^2}}. \tag{3}$$

According to the above Equation (3), the amplitude of output voltage is inversely proportional to the frequency f, the resistor R, and the capacitor C. Note that the amplitude directly reflects the fluctuation of the output pressure in the pressure-driven flow setup; the amplitude of output pressure is totally dependent on the above three factors.

As in a traditional RC low-pass filter, the resistor R is chosen having a constant resistance; thus, the effect of the resistor on the amplitude of output pressure is permanent. However, due to the application of the microfluidic gas damper with varied resistance in the setup, the resistance of the damper is directly influenced by the input gas pressure and is varied with the variation of input pressure. Therefore, the amplitude of output pressure is strongly determined by the damper. Since the time constant in the RC low-pass filter reflects the damping capability of the setup, in order to examine the pressure damping functionality of the gas damper, we tested and compared the time constants of the setup that included a gas damper (Type B in Table S1, supplementary material) or a constant resistor under the fixed input pressures (Figure 1(e)). To make a fair comparison, the resistor was fabricated having the same dimensions with the damper but with no elastic membranes. The capacity of the reservoir was 135 ml, and 125 ml deionized water was filled in the reservoir which left a gas volume of 10 ml. To make sure the reservoir was totally sealed, the outlet of reservoir was blocked. In the experiment, the input test pressure was gradually increased from 1 kPa to 100 kPa. The recorded curves of time constants show that when the test pressure is lower than 20 kPa, the setup with a damper or a resistor achieves nearly the same time constant values. However, with the continuously increase of test pressure, the setup with a damper needs more time to achieve the stable pressure output than the setup with a resistor. It can be concluded that the gas damper shows stronger pressure damping capability than the resistor at higher input pressures. It is worth noting that although at higher test pressures the setup with a damper requires a longer time to maintain a constant pressure, the time constant was found to be less than 1 min.

We also tested the output pressures under varied input pressures at an open-loop setup where the outlet of reservoir was unblocked; thus, the output pressure could pump the deionized water out (Figure 2). The input pressures were set to be varied according to the sinusoidal wave with a pulsation frequency of 0.5 Hz, and the gas volume was still set to be 10 ml. The obtained profiles of input and output pressures in Figure 2(a) show that the employment of either the damper or the resistor effectively decreases the pressure fluctuations of the input gas, and the amplitudes of the input pressures are also significantly reduced. However, with the increase of the input pressure, we found that the pressure variation produced by the resistor is far higher than that generated by the damper (Figure 2(b)). At input pressures of 10–100 kPa, the calculated normalized amplitude of the resistor is ~283.3% higher than that of the damper (Figure 2(c)). We think that this amplitude deviation is due to the significant difference in pneumatic resistance between the damper and the resistor. As demonstrated in the design concept, the pneumatic resistance of the damper increases at higher input pressures while the resistor maintains its resistance constant regardless of pressure variation. According to the Equation (3) of the RC low-pass filter model, the damper would obtain a lower amplitude than the resistor. Therefore, the installation of a damper in the pressure-driven flow setup is beneficial for generating highly stable pressures.

B. Effects of gas volume and pressure frequency

The gas volume within the sample reservoir is an important factor influencing the amplitude of output pressure in the pressure-driven flow setup. Similar to a capacitor, the large-volume reservoir can store a large amount of gas and deliver pressure for a long time. In order to probe into the effects of gas volume on pressure fluctuation, we measured the damped pressures under five different gas volumes from 2 ml to 120 ml, as shown in Figure 3. We found that the amplitude of the output pressure decreases gradually with the increase of the gas volume under all input pressures. A quantitative analysis of the relative variation of amplitude demonstrates that the pressure fluctuations can be further diminished at larger gas volumes. Although highly stable pressure can be obtained under large gas volumes, the contained sample

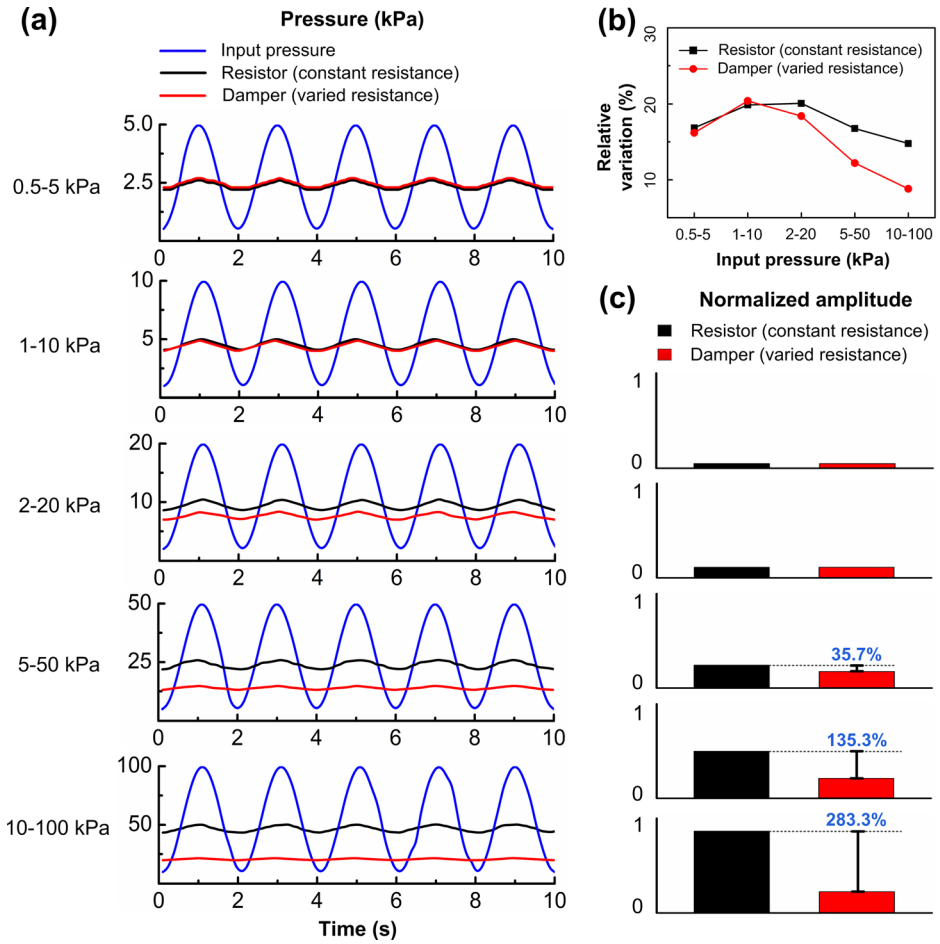

FIG. 2. Characterization of pressure fluctuations output by the pressure-driven setup with a resistor or a damper. (a) Comparisons of the pressure profiles produced by a damper with varied resistance and the pressure profiles by a constant resistor without membranes under different input pressures of 0.5–5 kPa, 1–10 kPa, 2–20 kPa, 5–50 kPa, and 10–100 kPa, respectively. The pulsation frequency of the input pressure was set to be 0.5 Hz, and the gas volume of the sample reservoir was 10 ml. (b) Pressure variation as a function of input pressure. (c) Comparison of normalized amplitudes of the resistor and the damper.

fluid in the reservoir is reduced accordingly. Moreover, the increased gas volume also requires a large-capacity reservoir, which directly influences the final footprint of the integrated microfluidic system. Instead, we found, from the results at a minimal volume of 2 ml gas, that the pressure variations are higher than 25% under most input pressures, which demonstrates that the extremely small gas chamber size is not enough for effectively removing the pressure fluctuations of the setup. We also measured the output flow rates of the pressure-driven flow setup under the above experimental conditions. The flow-rate profiles illustrated in Figure S2 (supplementary material) show that under all test pressures the output flow rates remain nearly unchanged with varying gas volumes, which indicates that the flow rate is not affected by the gas volume of the reservoir during the sample consumption process. Based on the above experimental findings, a gas chamber size of 10 ml was selected for the following tests and applications as this chamber size captures a relatively good damping effectiveness while the size is acceptable in practical microfluidic systems.

We next investigated the effects of input pressure frequency on the pressure fluctuation of the output gas. As the pulsation frequency of input pressure refers to the fill time and the amount of the gas stored in the sample reservoir, it affects the output pressure directly. We set the input pressures to be varied at four different frequencies of 0.25 Hz, 0.5 Hz, 1 Hz, and 5 Hz. The gas volume of the sample reservoir was chosen to be 10 ml. The quantitative analysis of

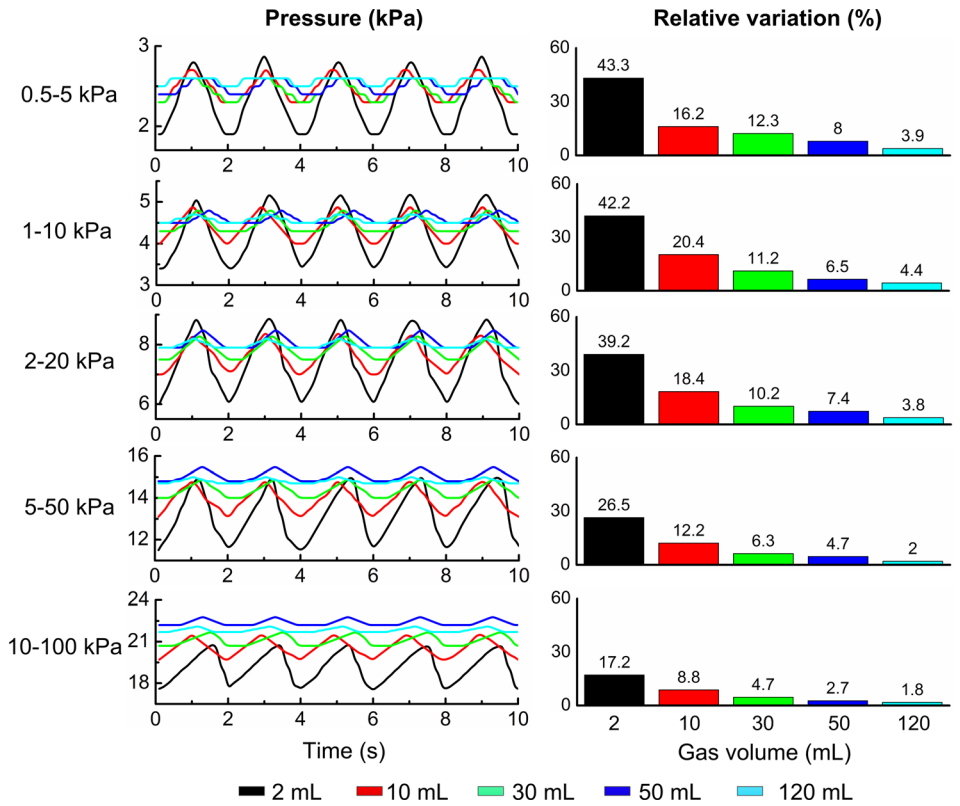

FIG. 3. Effects of gas volume on output pressure fluctuation under different input pressures with a pulsation frequency of 0.5 Hz. Pressure profiles were obtained at five different gas volumes of 2 ml, 10 ml, 30 ml, 50 ml, and 120 ml. The relative pressure variation was defined as the ratio of the peak-to-peak pressure value to the mean value.

the amplitude and relative variation of the output pressures is shown in Figure 4. We found that when the pulsation frequency is increased from 0.25 Hz to 1 Hz, both the amplitude and the relative variation decrease very quickly. We also found that at the highest pulsation frequency of 5 Hz, the output pressures become completely stable as all of the amplitudes approach to be zero. It is noted that when the pulsation frequency is higher than 1 Hz, all of the amplitudes decrease to be less than 0.5 kPa and the relative variations are lower than 10%; thus, highly stable output pressure can be obtained in the pressure-driven flow setup.

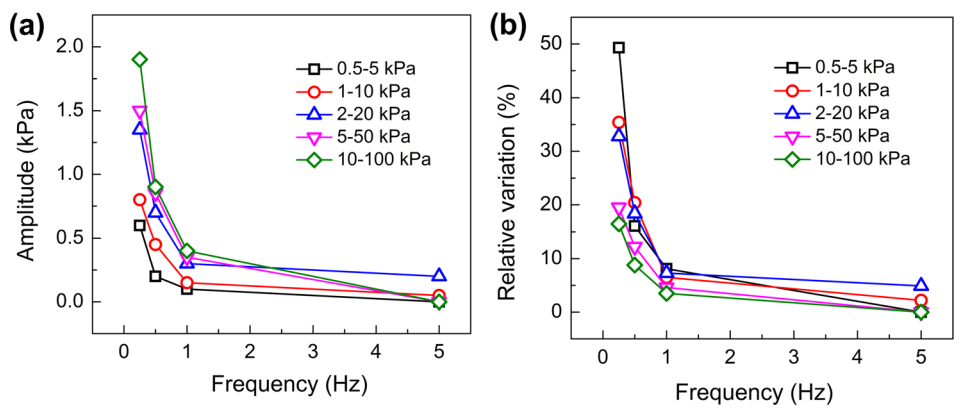

FIG. 4. Effects of the pulsation frequency of the input pressure on output pressure fluctuation. (a) Pressure amplitude versus frequency; (b) Relative pressure variation versus frequency. Pressure profiles were obtained at four different frequencies of 0.25 Hz, 0.5 Hz, 1 Hz, and 5 Hz. The gas volume of the sample reservoir is 10 ml.

Besides the effects of the above two factors (i.e., gas volume and pressure frequency), we also investigated the effects of fluidic resistance and sample liquid viscosity on the output pressure fluctuation. The experimental results show that both the fluidic resistance and viscosity have minimum effects on the output pressure (Figures S3 and S4, supplementary material). As a conclusion, our microfluidic gas damper shows a significant gas damping capability, and the model of the RC low-pass filter validates the applicability of the pressure-driven flow setup for providing stable fluid-pressures. Since the gas volume and the pressure frequency have a direct influence on the stabilization of the output pressure, a major consequence of the method is that as the gas volume or pressure frequency decreases, the stability of the output pressure deteriorates. Therefore, a good balance between the two factors is necessary for practical applications.

C. Low-cost and precise microfluidic injection application

To validate the practical application of our microfluidic gas damper, we designed a portable microfluidic system integrated with a gas damper to stabilize gas pressure for the smooth flow-rate delivery in the downstream. The schematic diagram of our portable pressure-driven flow system is shown in Figure 5(a). The system is composed of a small air blower, a microfluidic gas damper, and a centrifuge tube. Here, a hand-operated air blower with a maximum output gas pressure of ~45 kPa was employed as the portable pressure source. 5 ml deionized water was filled into the centrifuge tube, whose total capacity was 15 ml. In order to obtain flow rates of low and high-throughputs, a damper with strong damping capability (Type A in Table S1, supplementary material) and a damper with weak capability (Type C in Table S1, supplementary material) were, respectively, installed into the system. In addition, a microfluidic flow resistor was connected to the outlet of the centrifuge tube to constrain the fluidic resistance. To actuate the system, the air blower was periodically pressed by human fingers to produce a pulsed compressed air (CDA).

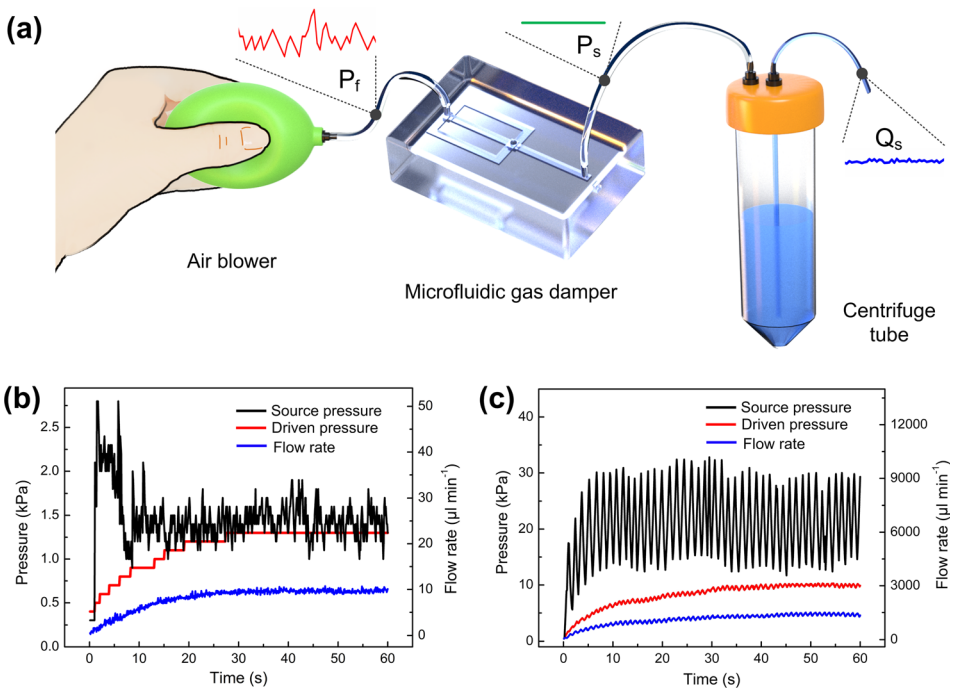

FIG. 5. Application of the microfluidic gas damper in the portable pressure-driven flow system for stable flow-rate delivery. (a) Schematic diagram of the pressure-driven system integrated with an air blower, a microfluidic gas damper, and a centrifuge tube. In the pressure-driven system, the pulsed gas pressures (P_f) produced by the air blower are damped by the gas damper, producing a stable driving pressure (P_s) which drives the sample fluids in the centrifuge tube and finally generates a precise fluidic flow rate (Q_c). (b) Stable driving pressure and low throughput flow rate generated by the pressure-driven system with a strong gas damping capability. (c) High-throughput fluid yielded by the pressure-driven system with a weak gas damping capability. The average flow rate was statistically processed as the mean ± standard error in a second.

The output air was then damped by the gas damper and stored in the centrifuge tube so that the deionized water could be consistently pushed out.

We first examined the damped pressure and the output flow rate in the system with a strong damping effect, as shown in Figure 5(b). Due to the strong pneumatic resistance induced by the damper, a limited and fluctuated gas pressure (less than 3 kPa) was produced by the air blower. In order to obtain a highly stable driving force under such a low pressure source, a finger-press frequency of ∼2 Hz was used to actuate the air blower periodically. The profile of the damped pressure shows that the fluid-driving pressure increases gradually at the beginning of the actuation process, and a constant value of 1.3 kPa is achieved after 30 s. The output flow rate of the system was also found to increase at first and then maintain a very small value of $\sim 9.64 \pm 0.27\ \mu l\,min^{-1}$ (average error of ∼2.8%). The working condition of the system with a weak damping effect was also characterized, as illustrated in Figure 5(c). The air blower was finger-pressed using an actuation frequency of ∼1 Hz, and the output flow rate with a mean value of $\sim 1367.15 \pm 78.21\ \mu l\,min^{-1}$ (average error of ∼5.7%) was achieved successfully.

The above experimental results well indicate that with the integration of a microfluidic gas damper and a centrifuge tube, the unstable compressed air produced by the air blow can be effectively damped and stabilized, and thus smooth flow rates with low or high-throughputs can be produced successfully. The significant advantage of our microfluidic gas damper is the total passiveness in gas damping, which means that high pulsed pressures can be automatically damped via the damper. We believe that our gas damper will be a good supplement to the existing peristaltic or pressure-driven micropumps. Due to the periodic variation of volumes in the deformable channel or chamber, these micropumps usually produce pulsed pressures, which also leads to the fluctuated flow rates in the downstream microfluidic devices.[35,38] As our gas damper is totally passive in pressure damping, the damper can be integrated with the peristaltic or pressure-driven micropumps directly; thus, pulsed pressures generated by the micropumps could be effectively damped and stable fluid delivery can be realized.

III. CONCLUSION

In conclusion, a novel microfluidic gas damper was proposed and installed to a pressure-driven flow system in this work for providing stable fluid-driving pressures in a low-cost and portable manner. The design mechanism of this method can be estimated as the equivalent electric circuit model of a RC low-pass filter, and the employment of the gas damper in the gas circuit can significantly decrease the amplitude of the output pressures. The experimental results demonstrate that the gas volume of the sample reservoir and the frequency of the pressure source have a direct influence on the output pressure. The practical application of our gas damper was examined through a portable microfluidic pressure-driven system in which the fluid-driving pressure was provided by a hand-operated air blower. Through a periodic pressing of the air blower by human fingers, smooth flow rates at both low and high-throughputs were generated successfully. Future integration of our gas damper with miniaturized pressure generators, such as peristaltic or pressure-driven micropumps, can be carried out to fully exploit its potential in low-cost microfluidic applications where highly stable pressures and flow controls are required.

IV. EXPERIMENTAL SECTION

A. Device design

A three dimensional (3D) architecture of five-layer stacking was designed in our microfluidic gas damper. The device contains two detour channel layers (see layers #1 and #5 in the right inset of Figure 1(a)), two thin membrane layers (layers #2 and #4), and a through channel layer (layer #3). These layers were designed and fabricated independently so that the device can be assembled through the complex combination of the differently sized layers, which permits a high freedom in the device optimization. In order to change the gas damping effects, a

narrow section in the middle of the through channel was designed with different widths. The detailed dimensions of the device are shown in Table S1 (supplementary material).

B. Device fabrication

The microfluidic gas damper was fabricated in PDMS (Slygard 184, Dow Corning) using the multilayer soft lithography technique.[22,36,37] It is noted that the elastic design of the damper membranes would allow large deformation even under low actuation pressures (Young's modulus of $\sim 266 \pm 47$ kPa), and thus the mixture of base and curing agent with a ratio of ~20:1 was applied.[32] The brief fabrication process of the gas damper can be divided into four steps (Figure S5, supplementary material). First, the detour channel layer was fabricated by patterning the PDMS (base to curing agent of 10:1) on a SU-8 master mold using the standard soft photolithography technique. Second, PDMS (base to curing agent of 20:1) was spun on a sheet of the CAPTON film, and it was cured to obtain a layer of thin membrane (curing time of ~15 min at the temperature of 80 °C). Then, the obtained detour channel layer was bonded onto the membrane and peeled off together with the membrane from the CAPTON film. Third, the through channel layer was fabricated by compressing the liquid PDMS (base to curing agent of 10:1) onto the surface of another master mold. After curing (100 °C for ~3 h), the part obtained in the second step was bonded together with the through channel layer. In the end, the other side of the part in the third step was aligned and bonded with the part in the second step to complete the device assembly. A photograph of the fabricated prototype damper is shown in the lower left corner of Figure S5.

C. Experimental setup

For constructing the pressure-driven flow setup, compressed air (CDA) was used to drive the sample fluid, and a commercial pressure controller (OB1 Base MkIII, Elveflow) was used to regulate the CDA to reach the designed pressures. The regulated gas then flowed through a microfluidic gas damper and a pressure sensor (Autonics, PSAN-C01CV-Rc1/8) in turn, and it was filled into a sealed sample reservoir. A flow sensor (MFS 4 & MFS 5, Elveflow) was used to measure the flow rate of the sample delivered by the reservoir. To constrain the flow resistance of the liquid circuit, a microfluidic flow resistor was installed in the downstream of the flow sensor.

D. Numerical simulation

The numerical simulations of pressure variation inside of the gas damper or the constant resistor were solved by the three dimensional (3D) Fluid-Structure Interaction (FSI) model using COMSOL Multiphysics®. In the FSI model, the PDMS membrane was selected as the linear elastic material, and the solid stress-strain model for the membrane was set a Young's modulus of 266 kPa with a Poisson's ratio of 0.49. In the fluid domain, atmosphere was assigned as the fluid material with a density of 1.293 kg m^{-3}.

SUPPLEMENTARY MATERIAL

See supplementary material for the numerical simulation model of the gas damper, the detailed dimensions of the employed three gas dampers, and additional experimental results illustrating the effects of fluidic resistance and viscosity on gas damping performance.

ACKNOWLEDGMENTS

This research work was supported by the National Natural Science Foundation of China (Grant Nos. 51505082 and 51375089), the Natural Science Foundation of Jiangsu Province (Grant No. BK20150606), the "333" Project of Jiangsu Province (Grant No. BRA2015291), the Open Foundation of the State Key Laboratory of Fluid Power and Mechatronic Systems (Grant No. GZKF-201501), and the Scientific Research Foundation of Graduate School of Southeast University (Grant No. YBPY1601).

[1]N. M. Karabacak, P. S. Spuhler, F. Fachin, E. J. Lim, V. Pai, E. Ozkumur, J. M. Martel, N. Kojic, K. Smith, P. I. Chen, J. Yang, H. Hwang, B. Morgan, J. Trautwein, T. A. Barber, S. L. Stott, S. Maheswaran, R. Kapur, D. A. Haber, and M. Toner, Nat. Protoc. **9**, 694 (2014).
[2]P. L. Voyvodic, D. Min, and A. B. Baker, Lab Chip **12**, 3322 (2012).
[3]T. Houssin, J. Cramer, R. Grojsman, L. Bellahsene, G. Colas, H. Moulet, W. Minnella, C. Pannetier, M. Leberre, A. Plecis, and Y. Chen, Lab Chip **16**, 1401 (2016).
[4]N. Xiang, H. Yi, K. Chen, D. Sun, D. Jiang, Q. Dai, and Z. Ni, Biomicrofluidics **7**, 044116 (2013).
[5]X. Zhang, D. Huang, W. Tang, D. Jiang, K. Chen, H. Yi, N. Xiang, and Z. Ni, RSC Adv. **6**, 9734 (2016).
[6]S. Song, M. S. Kim, and S. Choi, Small **10**(20), 4123 (2014).
[7]N. Mavrogiannis, M. Ibo, X. Fu, F. Crivellari, and Z. Gagnon, Biomicrofluidics **10**, 034107 (2016).
[8]M. E. Piyasena, R. Newby, T. J. Miller, B. Shapiro, and E. Smela, Sens. Actuators, B **141**, 263 (2009).
[9]D. C. Duffy, O. J. A. Schueller, S. T. Brittain, and G. M. Whitesides, J. Micromech. Microeng. **9**, 211 (1999).
[10]R. Safavieh and D. Juncker, Lab Chip **13**, 4180 (2013).
[11]L. Gervais and E. Delamarche, Lab Chip **9**, 3330 (2009).
[12]A. R. Abate and D. A. Weitz, Biomicrofluidics **5**, 14107 (2011).
[13]D.-b. Seo, Y. Agca, Z. C. Feng, and J. K. Critser, Microfluid. Nanofluid. **3**, 561 (2007).
[14]Y. K. Cho, J. G. Lee, J. M. Park, B. S. Lee, Y. Lee, and C. Ko, Lab Chip **7**, 565 (2007).
[15]G. Czilwik, T. Messinger, O. Strohmeier, S. Wadle, F. von Stetten, N. Paust, G. Roth, R. Zengerle, P. Saarinen, J. Niittymaki, K. McAllister, O. Sheils, J. O'Leary, and D. Mark, Lab Chip **15**, 3749 (2015).
[16]S. Z. Razzacki, P. K. Thwar, M. Yang, V. M. Ugaz, and M. A. Burns, Adv. Drug Delivery Rev. **56**, 185 (2004).
[17]W. M. Saltzman and W. L. Olbricht, Nat. Rev. Drug Discovery **1**, 177 (2002).
[18]S. Nagrath, L. V. Sequist, S. Maheswaran, D. W. Bell, D. Irimia, L. Ulkus, M. R. Smith, E. L. Kwak, S. Digumarthy, A. Muzikansky, P. Ryan, U. J. Balis, R. G. Tompkins, D. A. Haber, and M. Toner, Nature **450**, 1235 (2007).
[19]Y. Chen, P. Li, P. H. Huang, Y. Xie, J. D. Mai, L. Wang, N. T. Nguyen, and T. J. Huang, Lab Chip **14**, 626 (2014).
[20]X. Mu, W. Zheng, J. Sun, W. Zhang, and X. Jiang, Small **9**, 9 (2013).
[21]X. Li, D. R. Ballerini, and W. Shen, Biomicrofluidics **6**, 11301 (2012).
[22]M. A. Unger, H.-P. Chou, T. Thorsen, A. Scherer, and S. R. Quake, Science **288**, 113 (2000).
[23]J. Kan, Z. Yang, T. Peng, G. Cheng, and B. Wu, Sens. Actuators, A **121**, 156 (2005).
[24]A. K. Au, H. Lai, B. R. Utela, and A. Folch, Micromachines **2**, 179 (2011).
[25]K. W. Oh and C. H. Ahn, J. Micromech. Microeng. **16**, R13 (2006).
[26]D. J. Laser and J. G. Santiago, J. Micromech. Microeng. **14**, R35 (2004).
[27]C. Zhang, D. Xing, and Y. Li, Biotechnol. Adv. **25**, 483 (2007).
[28]T. Thorsen, S. J. Maerkl, and S. R. Quake, Science **298**, 580 (2002).
[29]W. H. Grover, A. M. Skelley, C. N. Liu, E. T. Lagally, and R. A. Mathies, Sens. Actuators, B **89**, 315 (2003).
[30]I. E. Araci and S. R. Quake, Lab Chip **12**, 2803 (2012).
[31]X. Zhang, N. Xiang, W. Tang, D. Huang, X. Wang, H. Yi, and Z. Ni, Lab Chip **15**, 3473 (2015).
[32]I. Doh and Y. H. Cho, Lab Chip **9**, 2070 (2009).
[33]E. P. Kartalov, C. Walker, C. R. Taylor, W. F. Anderson, and A. Scherer, Proc. Natl. Acad. Sci. U.S.A. **103**, 12280 (2006).
[34]S. Begolo, D. V. Zhukov, D. A. Selck, L. Li, and R. F. Ismagilov, Lab Chip **14**, 4616 (2014).
[35]K. Iwai, K. C. Shih, X. Lin, T. A. Brubaker, R. D. Sochol, and L. Lin, Lab Chip **14**, 3790 (2014).
[36]Y. Xia and G. M. Whitesides, Annu. Rev. Mater. Sci. **28**, 153 (1998).
[37]B.-H. Jo, L. M. V. Lerberghe, K. M. Motsegood, and D. J. Beebe, J. Microelectromech. Syst. **9**, 76 (2000).
[38]P. Skafte-Pedersen, D. Sabourin, M. Dufva, and D. Snakenborg, Lab Chip **9**, 3003 (2009).